Mode identification and seismic study of δ Scuti, the prototype of a class of pulsating stars

J. Daszyńska-Daszkiewicz [©],[1]⋆ A. A. Pamyatnykh,[2] P. Walczak [©],[1] G. Handler,[2] A. Pigulski [©][1] and W. Szewczuk [©][1]

[1]*Instytut Astronomiczny, Uniwersytet Wrocławski, Kopernika 11, PL-51-622 Wrocław, Poland*
[2]*Nicolaus Copernicus Astronomical Center, Polish Academy of Sciences, Bartycka 18, PL-00-716 Warsaw, Poland*

ABSTRACT

We present a seismic study of δ Scuti based on a mode identification from multicoulor photometry. The dominant frequency can be associated only with a radial mode and the second frequency is, most probably, a dipole mode. The other six frequencies have more ambiguous identifications. The photometric mode identification provided also some constraints on the atmospheric metallicity [m/H] $\approx +0.5$ and microturbulent velocity $\xi_t \approx 4$ km s^{-1}. For models reproducing the dominant frequency, we show that only the fundamental mode is possible and the first overtone is excluded. However, the location of δ Scuti near the terminal age main sequence requires the consideration of three stages of stellar evolution. For the star to be on the main sequence, it is necessary to include overshooting from the convective core with a parameter of at least $\alpha_{ov} = 0.25$ at the metallicity greater than $Z = 0.019$. It turned out that the value of the relative amplitude of the bolometric flux variations (the non-adiabatic parameter f) is mainly determined by the position of the star in the HR diagram, i.e. by its effective temperature and luminosity, whereas the effect of the evolutionary stage is minor. On the other hand, the convective efficiency in the subphotospheric layers has a dominant effect on the value of the parameter f. Comparing the theoretical and empirical values of f for the radial dominant mode, we obtain constraints on the mixing length parameter α_{MLT} which is less than about 1.0, independently of the adopted opacity data and chemical mixture. This value of α_{MLT} is substantially smaller than for a calibrated solar model indicating rather low to moderately efficient convection in the envelope of δ Scuti.

Key words: stars: evolution – stars: individual: δ Scuti – stars: oscillation.

1 INTRODUCTION

δ Scuti stars are classical pulsators with masses in the range of about 1.6–2.6 M$_\odot$. Most of them are in the main-sequence phase of evolution but there are δ Sct stars that have already completed central hydrogen burning (e.g. Breger & Pamyatnykh 1998; Bowman et al. 2016) or δ Sct stars in the pre-main-sequence contraction stage (e.g. Marconi & Palla 1998; Zwintz et al. 2014). The pulsational driving mechanism of these variables has been understood a long time ago (Chevalier 1971). This instability is due to the opacity mechanism operating in the second helium ionization zone but there may also be a small contribution to driving from the hydrogen ionization region (Pamyatnykh 1999). Radial pulsations and non-radial pulsations in pressure (p) and gravity (g) modes can be excited.

In most δ Scuti stars multiperiodicity is observed which potentially permits the derivation of stringent seismic constraints on their internal structure and evolution. Before the era of space-based observations of pulsating stars, the δ Sct star with the most detected pulsation frequencies was FG Vir (Breger et al. 2005), with almost 70 independent oscillation modes. The richness of the oscillations of

the δ Sct variables was revealed by the satellite missions CoRoT and Kepler. For some objects hundreds of frequencies were extracted from the light curves. For example, the CoRoT observations of HD 50844 revealed hundreds of peaks in the frequency range 0–30 d^{-1} (Poretti et al. 2009). In particular, the detection of high-order g modes in most δ Scuti stars observed by Kepler (Grigahcéne et al. 2010) required a new approach to pulsational modelling because such modes are stable in all stellar models computed with the standard opacity data (Balona, Daszyńska-Daszkiewicz & Pamyatnykh 2015). Using *Gaia* DR2 parallaxes and Kepler data for a sample of over 15 000 A- and F-type stars, Murphy et al. (2019) classified them into δ Scuti and non-δ Scuti stars finding that many stars in the classical instability strip do not pulsate. They defined a new empirical instability strip in the Hertzsprung–Russell diagram that is systematically hotter than the theoretical strip. Bowman & Kurtz (2018) also found that a significant fraction of main-sequence δ Scuti stars is located outside of the classical instability strip in the HR diagram. To explain both low- and high-order pressure modes in δ Scuti stars, the mass dependence of the convective mixing length parameter may be important. A list of δ Scuti variable star candidates from the K2 mission as targets for asteroseismic studies was prepared by Guzik, Garcia & Jackiewicz (2019). Antoci et al. (2019) classified

⋆ E-mail: daszynska@astro.uni.wroc.pl

and studied pulsation properties of a sample of 117 δ Scuti and γ Doradus stars observed by the *TESS* mission. In particular, they stressed the important role of mixing processes in the outer stellar layers on pulsation driving.

Detailed seismic modelling of δ Scuti stars, in particular those observed from space, is hampered by a lack of mode identification. Except for a few cases of stars with some regular patterns in oscillation spectra, unambiguous identification of modes comes only from ground-based photometric and/or spectroscopic data. However, not all frequency peaks observed from space are detectable from the ground. Moreover, in δ Sct star models, the photometric amplitudes and phases are very sensitive to the efficiency of convective transport in the outer layers. This sensitivity occurs via the non-adiabatic parameter *f* that gives the relative amplitude of the radiative flux perturbation at the photospheric level. To by-pass this effect, Daszyńska-Daszkiewicz, Dziembowski & Pamyatnykh (2003) invented the method of simultaneous determination of the mode degree ℓ and the parameter *f* from multicolour data. Thinking the other way, one can expect constraints on the efficiency of envelope convection from a comparison of the theoretical and empirical values of *f*. Such constraints have been derived for several δ Scuti stars (Daszyńska-Daszkiewicz et al. 2003, 2005a; Daszyńska-Daszkiewicz 2007), and, recently, for SX Phoenicis, the prototype of Population II counterparts of δ Sct stars (Daszyńska-Daszkiewicz et al. 2020). The general conclusion was that convective transport in the envelope of SX Phe is poor to moderately efficient.

Here, we present the first mode identification based on multicolour photometry for the prototype star δ Scuti. In Section 2, we give brief description and literature survey for the star. Section 3 contains details of observations and frequency analysis. In Section 4, we present the mode identification based on the photometric amplitudes and phases. Pulsational models reproducing the dominant frequency are discussed in Section 5. Complex seismic modelling and discussions of various effects on the parameter *f* are given in Section 6. The summary and some conclusions are in the last section.

2 THE PROTOTYPE δ SCUTI

The class prototype δ Scuti (HD 172748) has a brightness $V = 4.71$ mag and a spectral type F2II-III (Gray, Napier & Winkler 2001). Its variable radial velocity was detected over 120 yr ago by Campbell & Wright (1900). δ Scuti is a quite nearby object with a *Gaia* EDR3 parallax $\pi = 16.1899$ (1157) mas translating into a distance $d = 61.8(4)$ pc (Gaia Collaboration 2021). There are several determinations of its effective temperature in the literature ranging from about 6770 K (Erspamer & North 2003) to about 7260 K (e.g. Balona 1994). The most recent determinations amount to $T_{\rm eff} \approx 7000$ K (e.g. Yushchenko et al. 2005; Holmberg, Nordstrom & Andersen 2009; Boeche & Grebel 2016). The surface gravity of δ Scuti is $\log g \approx 3.5$ (Erspamer & North 2003; Yushchenko et al. 2005). In our study, we allow for a whole range of $T_{\rm eff}$, i.e. 6770–7260 K, with a logarithmic value $\log T_{\rm eff} = 3.845(15)$.

According to Yushchenko et al. (2005), the metallicity of δ Sct is above the solar value and its abundance pattern is similar to those of Am-Fm type stars. Erspamer & North (2003) classified δ Sct among metallic giants, which they defined as evolved giants with a surplus of such elements as Al, Ca, Ti, Cr, Mn, Fe, Ni, and Ba. In the case of δ Scuti, all of these elements, except Ca, show an excess comparing to the solar values. The estimated values of metallicity in the literature are [Fe/H] = 0.41, by Holmberg et al. (2009) from the calibration of *uvbyβ* photometry, and [m/H] ∈ (0.18, 0.38) by Boeche & Grebel (2016) from spectroscopic analysis adopting
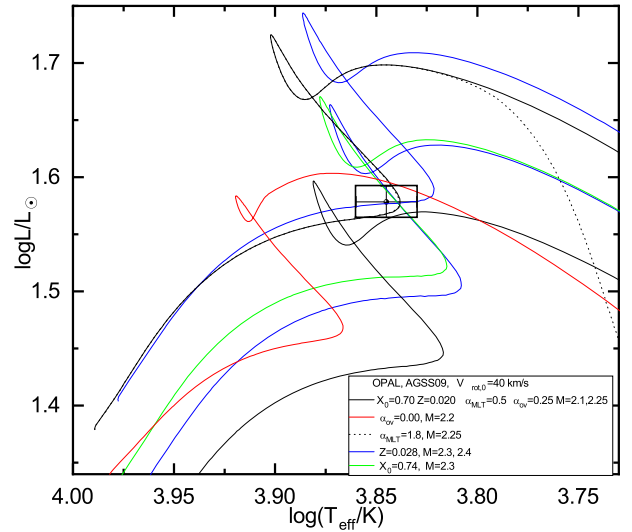

Figure 1. The HR diagram with the position of δ Scuti as determined from the whole observed range of the effective temperature and luminosity. The evolutionary tracks were computed for OPAL opacities with the AGSS09 solar mixture at various combinations of the initial hydrogen abundance X_0, metallicity Z, overshooting from the convective core $\alpha_{\rm ov}$, and the mixing length parameter in the envelope $\alpha_{\rm MLT}$, as indicated in the legend.

solar abundances of Grevesse & Sauval (1998). The microturbulent velocity of 2.8 km s^{-1} is given by Erspamer & North (2003) and 3.8 km s^{-1} by Yushchenko et al. (2005). If the inclination of the rotation axis is not low, δ Sct is a rather slow rotator with a projected rotational velocity $V_{\rm rot} \sin i = 25$ km s^{-1} (Erspamer & North 2003; Schroeder, Reiners & Schmitt 2009).

Using the *Gaia* EDR3 parallax and the bolometric correction from Kurucz models with a proper zero-point, i.e. $M_{\rm bol, \odot} = 4.62$ (Torres 2010), we derived the luminosity considering three values of the atmospheric metallicity [m/H] = 0.2, 0.3, 0.5 and the microturbulent velocity $\xi_t = 2$ km s^{-1}. Unfortunately, there are no Kurucz models for [m/H] = 0.4 and for higher values of ξ_t at the metallicity [m/H] $\geq$ 0.2. We obtained the following values: $\log L/L_\odot = 1.584(12)$ for [m/H] = 0.2, $\log L/L_\odot = 1.580(12)$ for [m/H] = 0.3, and $\log L/L_\odot = 1.574(13)$ for [m/H] = 0.5. For the further studies, we adopted the total range that is $\log L/L_\odot = 1.578(17)$.

To convert the metallicity [m/H] into the metal mass fraction Z, one can use a simple approximate formula

$$[\text{m/H}] = \log(Z/Z_\odot) - \log(X/X_\odot).$$

The value of [m/H] ∈ (0.18, 0.38), as determined by Boeche & Grebel (2016), translates into $Z = 0.031 \pm 0.07$ at $X = 0.70$, taking the values of $X_\odot = 0.7345$ and $Z_\odot = 0.0169$ from Grevesse & Sauval (1998). However, one has to be aware that the chemical anomalies are observed in the atmosphere of δ Scuti and the bulk metallicity of the star can be much lower or even around the solar value. Therefore, in our analysis we will consider also lower values of Z than those obtained above.

The position of δ Scuti in the HR diagram is shown in Fig. 1. The evolutionary tracks were computed using the Warsaw–New Jersey code (e.g. Pamyatnykh et al. 1998; Pamyatnykh 1999) assuming the OPAL opacity tables (Iglesias & Rogers 1996) and the opacities of Ferguson et al. (2005) for temperatures $\log T < 3.95$. In all calculations the solar chemical mixture was adopted from Asplund et al. (2009) (AGSS09) and the OPAL2005 equation of state was used (Rogers, Swenson & Iglesias 1996; Rogers & Nayfonov 2002). The

Warsaw–New Jersey code takes into account the mean effect of the centrifugal force, assuming solid-body rotation and constant global angular momentum during evolution. The treatment of convection relies on the standard mixing-length theory.

We depicted the tracks for masses in the range [2.1, 2.4] $M_\odot$ considering different values of the initial hydrogen abundance X_0 = 0.70, 0.74, metallicity Z = 0.020, 0.028, overshooting from the convective core α_{ov} = 0.0, 0.25 and the mixing length parameter for envelope convection α_{MLT} = 0.5, 1.8, to demonstrate the effects of these parameters. In all cases the initial rotational velocity of V_{rot} = 40 km s^{-1} was assumed to reach the value of about 25–30 km s^{-1} within the error box of the position of δ Scuti in the HR diagram.

As one can see, the star is located around the Terminal Age Main Sequence (TAMS), which means that three evolutionary phases have to be considered: main sequence (MS), overall contraction (OC), and post-MS. To consider δ Scuti models in the MS phase, convective overshooting of at least α_{ov} = 0.25 is indispensable.

Despite being the prototype of the class, δ Scuti has so far been insufficiently observed and studied. Up to now six frequencies were detected in its light curve in the range 4.6–8.6 d^{-1} by Templeton et al. (1997) who carried out a 5-yr Strömgren y photometric campaign. Moreover, Templeton et al. (1997) constructed a grid of evolutionary and non-adiabatic pulsational models. For their best-fitting models, they associated the highest amplitude frequency ν_1 = 5.16 d^{-1} with the radial fundamental mode in contrast to the results of Balona, Dean & Stobie (1981) and Cugier & Monier (1993) that the strongest mode is the radial first overtone. Furthermore, Templeton et al. (1997) obtained that all modes with frequencies in the observed range are unstable. However, without observations in more passbands an independent mode identification was impossible. Cugier & Monier (1993) used the phase shifts between radial velocity data and light curves obtained from *IUE* and infrared data in order to identify the modes. Their preliminary mode identification for the second frequency ν_2 = 5.35 d^{-1} was a ℓ = 2, p_2 mode. Apart from the works of Templeton et al. (1997) and Cugier & Monier (1993), there were no more studies of the properties of the pulsational modes of δ Scuti.

3 SPACE AND GROUND-BASED PHOTOMETRY

As mentioned above, Templeton et al. (1997) carried out a photometric campaign observing δ Scuti in the years 1983–1988 in the Strömgren y filter. They discovered eight terms in their photometry, including six independent frequencies, one harmonic of the strongest frequency, and one combination frequency. Their data suffered from strong daily and yearly aliasing, leaving some ambiguity in the frequencies of all but the two strongest peaks. In this paper, we analyse the three photometric data sets. First, we use Solar Mass Ejection Imager (SMEI) space wide-band photometry to derive precise frequencies of pulsations. Then, the Strömgren uvy ground-based data gathered by us at Fairborn Observatory are analysed to obtain multiband amplitudes and phases of the observed frequencies. Finally, we reanalyse y-filter photometry of Templeton et al. (1997).

3.1 SMEI photometry

The SMEI experiment placed aboard the Coriolis spacecraft (Eyles et al. 2003; Jackson et al. 2004) measured sunlight scattered by free electrons in the solar wind scanning the whole sky with three wide-field cameras. A by-product of the mission was time-series photometry of over 5500 bright stars obtained in the years 2003–2010. The SMEI photometry is affected by long-term calibration effects, especially a repeatable variability with a period of 1 yr. The

raw SMEI photometry of δ Sct, downloaded from the University of California San Diego (UCSD) web page,[1] was corrected for the 1-yr variability by subtracting an interpolated mean light curve. The mean light curve was obtained by folding the raw data with the period of 1 yr, calculating median values in 200 intervals in phase, and then interpolating between them. The interpolated curve was then subtracted from the data. The subsequent procedure was aimed at further removal of instrumental effects and consisted of the following steps: (i) Identification of the strongest frequencies in the frequency spectrum. (ii) Fitting a model consisting of a sum of sinusoids with the detected frequencies to the data and subtraction of this model from the data. The next three steps were carried out using residuals from this fit. (iii) Identification and rejection of outliers by means of the Generalized Extreme Studentized Deviate algorithm (Rosner 1983). (iv) Calculation of individual uncertainties using the scatter of the neighbouring data. The data with uncertainties higher than a subjectively chosen threshold were then removed from the data set. (v) Removal of low-frequency signals, primarily of instrumental origin, by the calculation of means in time intervals, interpolating between them and subtracting. Steps (iii) to (v) were iterated several times, yielding 22 795 data points that were used in the final analysis. The final uncertainties ranged between 5 and 25 mmag.

Analysis of the SMEI time-series photometry corrected for instrumental effects resulted in detection of 18 terms. We applied a standard prewhitening procedure, in which frequency spectra were calculated at each step with the use of a Discrete Fourier Transform. At each step of the procedure, all previously detected terms were added to the model consisting of a sum of sinusoidal terms. Their amplitudes and phases were derived by fitting the model to the original data by means of the least squares method. In the next step, the residuals from the fit were used to calculate the next frequency spectrum. Frequency spectra at several steps of prewhitening are shown in Fig. 2. Of all detected terms, 14 represent independent frequencies, two are harmonics of the highest amplitude frequency, ν_1, and the remaining two are combination frequencies. The frequencies and amplitudes of all terms are listed in Table 1.

As can be seen in Fig. 2 and Table 1, the independent frequencies extracted from the SMEI data occur in three relatively narrow ranges: between 4.74 and 5.35 d^{-1} (6 peaks), between 8.29 and 8.80 d^{-1} (6 peaks), and near 11.6 d^{-1} (2 peaks). A sudden drop of signal below ~0.7 d^{-1} and its replicas around the satellite's orbital frequency f_{orb} = 14.172 d^{-1} (Fig. 2) are the result of the strong detrending applied to remove the instrumental effects. If some low-amplitude peaks would be present at these frequencies, they would escape detection.

3.2 APT photometry

The star was also observed photometrically with the 0.75-m T6 automatic telescope at Fairborn Observatory (Arizona, USA) in three passbands, u, v, and y, of the Strömgren photometric system. Two comparison stars, HD 173093 (V = 6.30 mag) and HD 174464 (V = 5.84 mag), were used. No intrinsic variability of any of those two stars was detected within a limit of 1.2 mmag in Fourier space in the range of the pulsation frequencies of the prime target. Observations started on 2018 May 12 and were gathered during 36 nights, covering the interval of about 46 d. In Fig. 3, we plot examples of light curves in all three photometric bands.

The analysis of the APT data was carried out independently for the three passbands. Since single-site APT data suffer from strong

---

[1] http://smei.ucsd.edu/new_smei/index.html

reported by them are slightly deviant from our solution. These were 54.82807 μHz (4.737145 d^{-1}), which differs from ν_7 by about 0.0020 d^{-1} and 99.44722 μHz (8.592240 d^{-1}), which is off by about 0.0042 d^{-1} from ν_5. This is the result of identifying an alias as the true frequency. This possibility was pointed out by Templeton et al. (1997), who wrote that frequencies of the lower amplitude peaks they detected could be in error by 0.016 to 0.058 μHz. This corresponds to 0.0014–0.0050 d^{-1}, in full accordance with the above differences. In addition to the eight confirmed terms, we also detected ν_{13}, one of the smallest amplitude frequency found in the SMEI data. Amplitudes of all nine terms detected in MTy data are given in Table 1.

A comparison of the frequency values (and their amplitudes) detected in the data of Templeton et al. (1997) with those found in the SMEI and APT data provides additional evidence of the changes of amplitudes of the independent frequencies. For example, the amplitude of ν_5 is much smaller in the MTy data than in the APT data. Despite similar detection thresholds, ν_6, ν_8, and ν_9 present in the APT data were not detected in the MTy data. On the other hand, the frequency ν_{15} was detected only in the MTy data. Its reality is demonstrated in Fig. 5, in which we show the frequency spectrum of MTy data freed from all frequencies detected in these data but ν_{15}. The strongest alias of this frequency is about 10 per cent weaker, which leaves little ambiguity as to the correctness of the frequency ν_{15}.

The detection of ν_{15} only in the MTy data and a lack of ν_{13} in the APT data is again a manifestation of the amplitude modulation that occurs quite often in δ Scuti variables (e.g. Breger & Pamyatnykh 2006; Bowman et al. 2016).

4 MODE IDENTIFICATION

Here, we use the method of mode identification which is based on simultaneous determination of the mode degree ℓ, the intrinsic mode amplitude ε, and the non-adiabatic parameter f for a given frequency (Daszyńska-Daszkiewicz et al. 2003, 2005a). This method consists in least-squares fitting of the calculated values of the complex photometric amplitudes to the observed ones. We regard the degree ℓ and associated complex values of f and ε as most probable if they minimize the differences between the computed and observed complex amplitudes. Then, the empirical values of f can be directly compared with predictions from linear computations of stellar pulsations.

Below, we repeat basic formulae to remind the meaning of ε and f. The standard formula for the relative local radial displacement of the surface element caused by a pulsational mode with the angular frequency ω is

$$\delta r(R, \theta, \varphi) = R \mathrm{Re}\{\varepsilon Y_\ell^m(\theta, \varphi) \mathrm{e}^{-\mathrm{i}\omega t}\}, \tag{1}$$

where Y_ℓ^m denotes a spherical harmonic with degree ℓ and azimuthal order m and G, M, R have their usual meanings. The corresponding changes of the bolometric flux, $\mathcal{F}_{\mathrm{bol}}$, are given by

$$\frac{\delta\mathcal{F}_{\mathrm{bol}}}{\mathcal{F}_{\mathrm{bol}}} = \mathrm{Re}\{\varepsilon f Y_\ell^m(\theta, \varphi) \mathrm{e}^{-\mathrm{i}\omega t}\}. \tag{2}$$

Equation (2) defines the complex parameter f as the ratio of the relative flux variation to the relative radial displacement of the surface.

Both ε and f may be regarded constant in the atmosphere, so we can use the static plane-parallel approximation. Thus, in the framework of linear theory of stellar pulsations, assuming the zero-rotation approach, the complex amplitude of the relative flux variation in a passband λ for a given pulsational mode can be written as follows
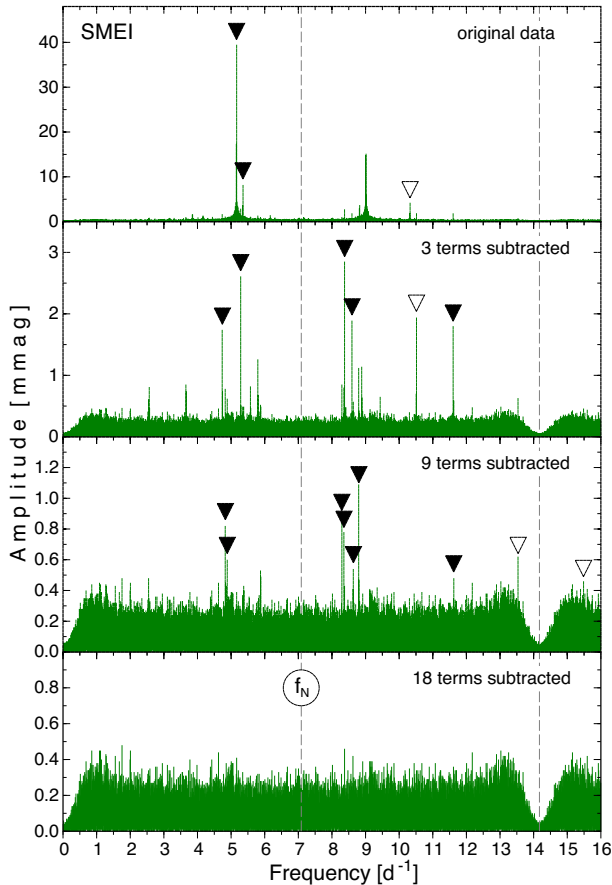

Figure 2. Fourier frequency spectra from the SMEI data. Going from top to bottom, the panels show four steps of prewhitening. The independent frequencies are shown with filled triangles, whereas the harmonics of ν_1 and combination frequencies with open triangles. The vertical dashed lines mark the satellite orbital frequency $f_{\mathrm{orb}} = 14.172$ d^{-1} and related Nyquist frequency $f_{\mathrm{N}} = f_{\mathrm{orb}}/2 = 7.086$ d^{-1}.

daily aliasing, during the consecutive steps of prewhitening the maxima with frequency equivalents obtained from the SMEI data were considered to be real. These were not always the highest peaks. The aliasing problem in the APT data is illustrated in Fig. 4, in which we show the frequency spectrum of the y-filter data after subtraction of the three strongest terms, ν_1, ν_2, and $2\nu_1$. The problem is compounded by the fact that frequencies of two terms, ν_5 and ν_6, are separated by almost exactly 3 d^{-1}, so that their daily aliases coincide. We detected the same 10 terms in all three passbands of the APT data; their amplitudes are given in Table 1. The detected terms were the strongest in the SMEI data, except for ν_3 that was not detected in the APT data. Such a huge amplitude drop, below the detection level, may be due to non-linear interaction of various pulsational modes (Moskalik 1985).

3.3 Reanalysis of Templeton et al.'s data

Having derived the frequencies from the SMEI data, we reanalysed the y-filter data published by Templeton et al. (1997) and kindly provided by Dr. Templeton. The data were obtained in the years 1983–1988 in three sites; we shall refer to them as to the 'MTy data'. Due to the large gaps in the data, they suffer from strong aliases as shown, for example, in their fig. 3. We recovered all eight frequencies listed in their Table 1. However, two of the frequencies

Table 1. Sinusoidal terms detected in the photometric data of δ Scuti. All frequencies but ν_{15} were detected in the SMEI data. Starting from the third column, the values of signal-to-noise ratio (S/N), semi-amplitude, A, and phase, ϕ, are given. The noise level in the frequency spectrum of residuals was calculated as a mean in the range 0–25 d^{-1} for the APT and MTy data and 1–13 d^{-1} for the SMEI data. Phases are given for the following epochs: HJD 2454000 for the SMEI data, HJD 2458270 for the APT data, and HJD 2446493.5 for the data of Templeton et al. (1997). Subscripts identify data set: SMEI data are labelled with 'SMEI', APT uvy data with 'u', 'v', and 'y', respectively, and y-filter data of Templeton et al. (1997), with 'y,T'. The final three rows of the table contain standard deviation of residuals, SDR, detection threshold, DT, defined as four times the noise level in the frequency spectrum of the residuals, and the number of observations used, N_{obs}. Numbers in parentheses represent uncertainties of the preceding values, with the leading zeroes omitted.

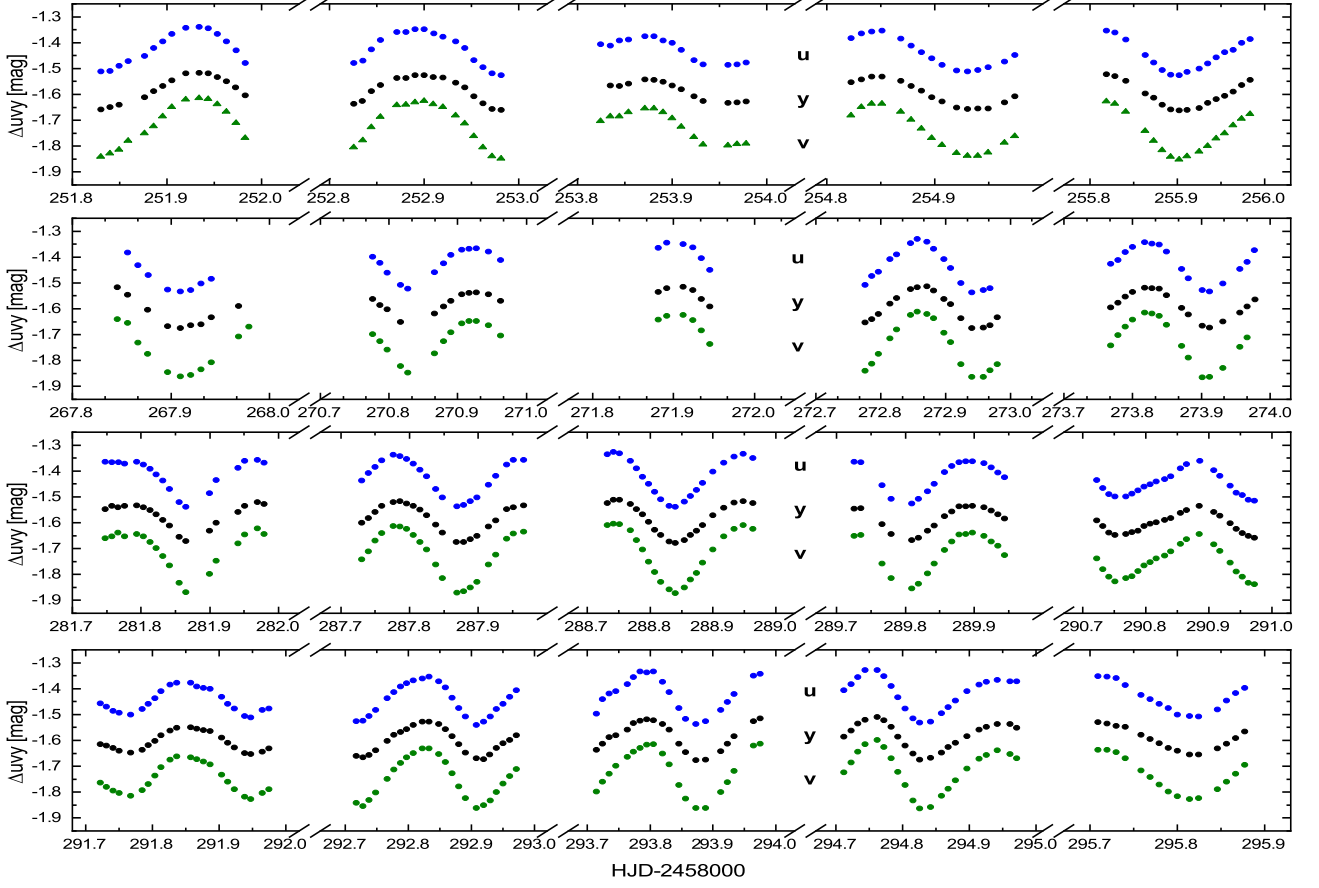| ID	Frequency [d^{-1}]	S/N (SMEI)	A_{SMEI} [mmag]	ϕ_{SMEI} [rad]	S/N (u)	A_u [mmag]	ϕ_u [rad]	S/N (v)	A_v [mmag]	ϕ_v [rad]	S/N (y)	A_y [mmag]	ϕ_y [rad]	S/N (y,T)	$A_{y,\text{T}}$ [mmag]	$\phi_{y,\text{T}}$ [rad]
ν_1	5.1607680(6)	357.8	39.64(12)	0.1109(29)	153.7	80.99(40)	3.238(5)	180.3	103.66(42)	3.184(4)	167.5	65.11(29)	3.129(5)	177.5	63.63(12)	4.5348(18)
ν_2	5.3512820(26)	76.7	8.50(12)	6.177(14)	34.6	18.24(41)	6.162(22)	41.6	23.94(43)	6.098(18)	38.2	14.85(30)	6.096(20)	39.3	14.08(12)	3.609(9)
$2\nu_1$	10.3215360	39.1	4.34(12)	2.754(27)	13.6	7.18(42)	2.67(6)	16.8	9.64(44)	2.56(5)	16.8	6.53(31)	2.51(5)	19.0	6.80(12)	5.309(18)
ν_3	8.376999(8)	25.5	2.83(12)	2.20(4)	–	–	–	–	–	–	–	–	–	–	–	–
ν_4	5.284892(9)	23.4	2.60(12)	4.63(5)	8.6	4.55(45)	1.62(10)	11.1	6.40(48)	1.43(8)	10.0	3.88(34)	1.61(9)	12.4	4.44(12)	3.524(28)
$\nu_1 + \nu_2$	10.5120499	17.5	1.94(12)	2.72(6)	7.7	4.07(40)	5.64(10)	9.5	5.49(43)	5.34(8)	8.9	3.46(30)	5.33(9)	9.5	3.40(12)	4.36(4)
ν_5	8.596409(13)	16.2	1.80(12)	4.62(7)	10.8	5.71(44)	2.71(8)	13.9	7.98(47)	2.45(6)	12.6	4.89(33)	2.50(7)	6.7	2.39(12)	5.16(5)
ν_6	11.603991(13)	16.1	1.78(12)	0.86(7)	10.2	5.36(44)	0.52(8)	10.7	6.13(47)	0.54(8)	9.7	3.76(33)	0.50(9)	–	–	–
ν_7	4.739179(13)	15.6	1.73(12)	0.02(7)	8.7	4.57(40)	1.99(9)	9.3	5.37(43)	1.87(8)	9.3	3.60(30)	2.05(8)	7.4	2.67(12)	2.04(5)
ν_8	8.799128(21)	9.7	1.07(12)	6.18(11)	9.3	4.90(40)	2.09(8)	12.2	7.04(42)	1.93(6)	11.5	4.45(30)	1.99(7)	–	–	–
ν_9	8.292173(25)	8.1	0.89(12)	3.93(13)	7.5	3.94(47)	5.81(12)	8.1	4.64(50)	5.73(11)	6.6	2.57(35)	5.76(14)	–	–	–
ν_{10}	4.828367(27)	7.5	0.83(12)	1.83(14)	–	–	–	–	–	–	–	–	–	–	–	–
ν_{11}	8.35574(3)	7.0	0.78(12)	2.52(15)	–	–	–	–	–	–	–	–	–	–	–	–
$\nu_1 + \nu_3$	13.537767	5.5	0.61(12)	5.70(19)	–	–	–	–	–	–	–	–	–	–	–	–
ν_{12}	4.88426(4)	5.5	0.61(12)	5.66(21)	–	–	–	–	–	–	–	–	–	–	–	–
ν_{13}	8.63759(5)	4.9	0.55(12)	1.95(24)	–	–	–	–	–	–	–	–	–	5.0	1.78(12)	0.06(7)
ν_{14}	11.62159(5)	4.4	0.49(12)	1.95(24)	–	–	–	–	–	–	–	–	–	–	–	–
$3\nu_1$	15.4823040	4.2	0.46(12)	5.28(25)	–	–	–	–	–	–	–	–	–	–	–	–
ν_{15}	8.3129127(7)	–	–	–	–	–	–	–	–	–	–	–	–	10.2	3.66(13)	5.20(4)
SDR [mmag]			12.35			6.50			6.68			4.65			6.39	
DT [mmag]			0.44			2.11			2.30			1.56			1.43	
N_{obs}			22795			558			564			559			6504	

Figure 3. Examples of the APT observations of δ Scuti in the Strömgren *uvy* passbands.
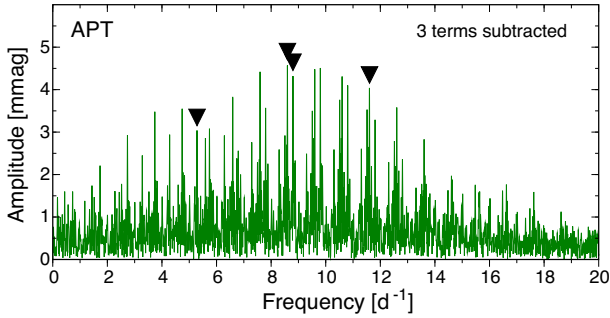

Figure 4. Fourier frequency spectrum of the *y*-filter APT data after subtracting the three strongest terms: ν_1, ν_2, and $2\nu_1$. The spectrum illustrates the problem of strong daily aliasing. The true frequencies of four fainter terms, ν_4, ν_5, ν_6, and ν_8, are indicated by inverted triangles.
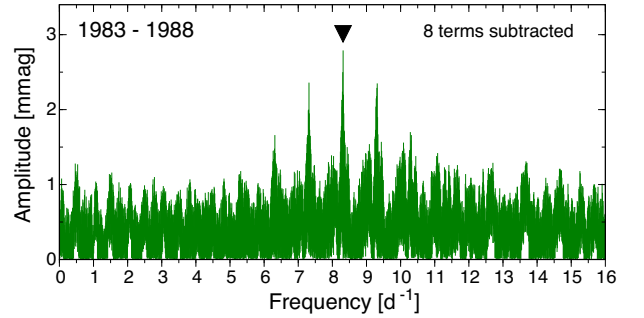

Figure 5. Fourier frequency spectrum from the *y*-filter data of Templeton et al. (1997) after subtraction of all terms detected in these data except for ν_{15}. The highest peak corresponding to ν_{15} is marked by the inverted triangle.

(e.g. Daszyńska-Daszkiewicz et al. 2003, 2005a):

$$\mathcal{A}^\lambda(i) = \mathcal{D}_\ell^\lambda(\tilde{\varepsilon} f) + \mathcal{E}_\ell^\lambda \tilde{\varepsilon}, \tag{3}$$

where

$$\tilde{\varepsilon} \equiv \varepsilon Y_\ell^m(i, 0), \tag{4a}$$

$$\mathcal{D}_\ell^\lambda = b_\ell^\lambda \frac{1}{4} \frac{\partial \log(\mathcal{F}_\lambda |b_\ell^\lambda|)}{\partial \log T_{\text{eff}}}, \tag{4b}$$

$$\mathcal{E}_\ell^\lambda = b_\ell^\lambda \left[(2+\ell)(1-\ell) - \left(\frac{\omega^2 R^3}{GM} + 2 \right) \frac{\partial \log(\mathcal{F}_\lambda |b_\ell^\lambda|)}{\partial \log g} \right], \tag{4c}$$

and

$$b_\ell^\lambda = \int_0^1 h_\lambda(\mu)\mu P_\ell(\mu)\mathrm{d}\mu. \tag{4d}$$

The term $\mathcal{D}_\ell^\lambda$ describes the temperature effects and $\mathcal{E}_\ell$ combines the geometrical and pressure effects. The partial derivatives of $\mathcal{F}_\lambda(T_{\text{eff}}, \log g)$ and $b_\ell^\lambda(T_{\text{eff}}, \log g)$ may be calculated numerically from tabular data. Their values depend also on the metallicity parameter [m/H] and microturbulent velocity ξ_t in the atmosphere. In this paper we use Vienna model atmospheres (Heiter et al. 2002) that include turbulent convection treatment from Canuto, Goldman & Mazzitelli (1996). Although the atmosphere of δ Scuti shows some

chemical peculiarity, as mentioned in Section 2, the abundances of elements with the atomic number $Z < 27$ are quite close to the solar values (Yushchenko et al. 2005). Moreover, here we do not analyse variations in single spectral lines but consider the light variations in the photometric passbands which have the width of about 200–300 Å. To give some quantitative measurement of the chemical peculiarity in the photometric bands, we calculated the peculiarity index Δp based on the Strömgren photometry as given by Masana et al. (1998). Using the photometric indices from Paunzen (2015) we got $\Delta p = 1.11$ which is lower than the threshold for normal stars of 1.50. Thus, it is reasonable to use the standard Vienna atmospheres for computations of the photometric amplitudes and phases of the δ Scuti pulsations.

For the limb darkening law, $h_\lambda(\mu)$, we computed coefficients assuming the non-linear, four-parametric formula of Claret (2000). The symbol i in equation (4a) means the inclination angle. To convert the flux amplitudes to magnitudes, the right-hand side of equation (3) must be multiplied by the factor (-1.086).

The goodness of the fit is obtained from the formula

$$\chi^2 = \frac{1}{2N - N_p} \sum_{i=1}^{N} \frac{\left| \mathcal{A}_{\lambda_i}^{obs} - \mathcal{A}_{\lambda_i}^{cal} \right|^2}{|\sigma_{\lambda_i}|^2}, \tag{5}$$

where N is the number of passbands λ_i and N_p is the number of parameters to be determined. The method yields two complex parameters, $\tilde{\varepsilon}$ and f, thus $M = 4$. The symbols $\mathcal{A}^{obs}$ and $\mathcal{A}^{cal}$ denote the complex observational and calculated amplitudes, respectively. The observational errors σ_λ are expressed as

$$|\sigma_\lambda|^2 = \sigma^2(A_\lambda) + A_\lambda^2 \sigma^2(\varphi_\lambda), \tag{6}$$

where $A_\lambda = |\mathcal{A}_\lambda|$ and $\varphi_\lambda = arg(\mathcal{A}_\lambda)$ are the values of the amplitude and the phase, respectively.

As has been mentioned in Section 2, the metallicity of δ Scuti is in the range of about [m/H] $\in$ (0.2, 0.4) and the microturbulent velocity in its atmosphere is about $\xi_t = 2.8$ km s^{-1}. In addition, the prototype has been classified as a chemically peculiar star because of an excess of some elements, e.g. iron, nickel, and manganese. Therefore, we consider three values of the atmospheric metallicity which are in the tabular data [m/H] = 0.2, 0.3, and 0.5 and two values of the microturbulent velocity $\xi_t = 2$ and 4 km s^{-1}, which gives six combinations of ([m/H], ξ_t). In Fig. 6, we plotted the values of χ^2 as a function of the mode degree ℓ for the dominant frequency $\nu_1 = 5.16077$ d^{-1} considering the six pairs of ([m/H], ξ_t) and the three values of the effective temperature $\log T_{\text{eff}} = 3.835$, 3.845, and 3.855 that cover the observed range. The value of luminosity in the adopted range, $\log L/L_\odot = 1.578(17)$, has only a minor effect on $\chi^2(\ell)$. The plotted values of the discriminant are for $\log L/L_\odot = 1.578$. As one can see, for all values of $\log T_{\text{eff}}$ and all pairs of ([m/H], ξ_t), a radial mode is strongly preferred. However, the run of $\chi^2(\ell)$ is very sensitive to the effective temperature as well as to the atmospheric parameters ([m/H], ξ_t). Even for fixed values of ([m/H], ξ_t) we have a very different dependence $\chi^2(\ell)$ for different values of $\log T_{\text{eff}}$. Only in the case of the metallicity [m/H] = 0.5 and microturbulent velocity $\xi_t = 4$ km s^{-1} the function $\chi^2(\ell)$ has a similar course for the three values of $\log T_{\text{eff}}$.

Because in case of radial modes $Y_\ell^m(i, 0) = 1$, our method gives an exact value of the intrinsic mode amplitude ε which for ([m/H], ξ_t) =(0.5, 4 km s^{-1}) is $\varepsilon = 0.006(3)$. This means that the pulsations of the dominant mode change the radius by 0.3–0.9 per cent at the photosphere level.

The amplitude of the radial velocity for a given pulsational mode can be estimated from the formula

$$\mathcal{A}(V_{\text{rad}}) = i\omega R \left(u_\ell^\lambda + \frac{GM}{R^3 \omega^2} v_\ell^\lambda \right) \tilde{\varepsilon}, \tag{7}$$

taking the empirical value of $\tilde{\varepsilon} = \varepsilon Y_\ell^m(i, 0)$ obtained from our method. The factors u_ℓ^λ and v_ℓ^λ are other integrals of the limb darkening law $h_\lambda(\mu)$

$$u_\ell^\lambda = \int_0^1 h_\lambda(\mu) \mu^2 P_\ell(\mu) \mathrm{d}\mu, \tag{7a}$$

$$v_\ell^\lambda = \ell \int_0^1 h_\lambda(\mu) \mu \left(P_{\ell-1}(\mu) - \mu P_\ell(\mu) \right) \mathrm{d}\mu, \tag{7b}$$

and are computed for the Strömgren passband y.

The latest determination of the radial velocity amplitudes for the pulsation frequencies of δ Scuti is due to Balona et al. (1981). They fitted all the published radial velocities using the two main frequencies and the first harmonic of the dominant one and obtained the amplitudes: $A_{\text{Vrad}} = 4.1(1)$ km s^{-1} for ν_1 and $A_{\text{Vrad}} = 1.8(1)$ km s^{-1} for ν_2. Our estimate for ν_1 calculated from equation (7) is about $A_{\text{Vrad}} = 4.8(2.6)$ km s^{-1} and it agrees within the errors with the value of Balona et al. (1981). Of course, the amplitudes could change within about 40 yr between the two data sets, but comparing the amplitude in the V filter of Balona et al. (1981) with our y amplitude we conclude that they agree within 2.5σ.

In Fig. 7, we presented the results of the ℓ identification for the second frequency $\nu_2 = 5.35128$ d^{-1}. The light amplitude of ν_2 is about 4.5 times smaller than the amplitude of the dominant frequency. In the case of ν_2, one can see even a greater dependence of the function $\chi^2(\ell)$ on the parameters ([m/H], ξ_t) and on T_{eff} and, most importantly, the uniqueness of the identification of ℓ depends on them. For most combinations of ([m/H], ξ_t) the degrees $\ell = 1$, 2, 3 are equally possible. As in the case of ν_1, a similar run of $\chi^2(\ell)$ for each T_{eff} is obtained for ([m/H], ξ_t) = (0.5, 4 km s^{-1}). For these parameters, we also obtain an unambiguous identification of the degree $\ell = 1$.

However, in order to definitely decide on the identification of ℓ for ν_2, we calculated the amplitude of the radial velocity according to equation (7). In Fig. 8, we show these empirical values of $A_{\text{Vrad}} = |\mathcal{A}(V_{\text{rad}})|$ as a function of ℓ, computed assuming the intrinsic amplitudes $\tilde{\varepsilon}$ as determined simultaneously with ℓ and the parameter f. All combinations of ([m/H, ξ_t]) depicted in Fig. 7 were considered and the same three values of T_{eff} were assumed. The horizontal lines mark the allowed observed range as determined by Balona et al. (1981). As one can see, only for a dipole mode our estimated values of A_{Vrad} reach the observed range for all values of the metallicity [m/H] and microturbulent velocity ξ_t. Thus, even though the radial velocity amplitude can slightly change, we conclude that an $\ell = 1$ mode is the most probable identification for frequency ν_2.

The discriminant $\chi^2(\ell)$ for the remaining six frequencies is plotted in Fig. 9, for the atmospheric parameters [m/H]=0.5, $\xi_t = 4$ km s^{-1} which gave the most homogeneous dependence of $\chi^2(\ell)$ on the effective temperature for ν_1 and ν_2. We remind that the frequency $\nu_3 = 8.376999$ d^{-1} was not detected in the APT data, therefore the photometric identification of the degree ℓ is not possible for it. As one can see in Fig. 9, the frequency $\nu_4 = 5.28489$ d^{-1} can be $\ell = 1$, 2, 3, or 5, however $\ell = 5$ is much less probable because its visibility is much lower. The frequency $\nu_5 = 8.59641$ d^{-1} is most probably a mode with $\ell = 1$ or 2. In the case of $\nu_6 = 11.60399$ d^{-1} we can exclude modes with $\ell > 4$ as well as a radial mode because there are no radial overtones in pulsational models with close frequencies. The most likely mode degrees for $\nu_7 = 4.73918$ d^{-1} are $\ell = 2$, 3,
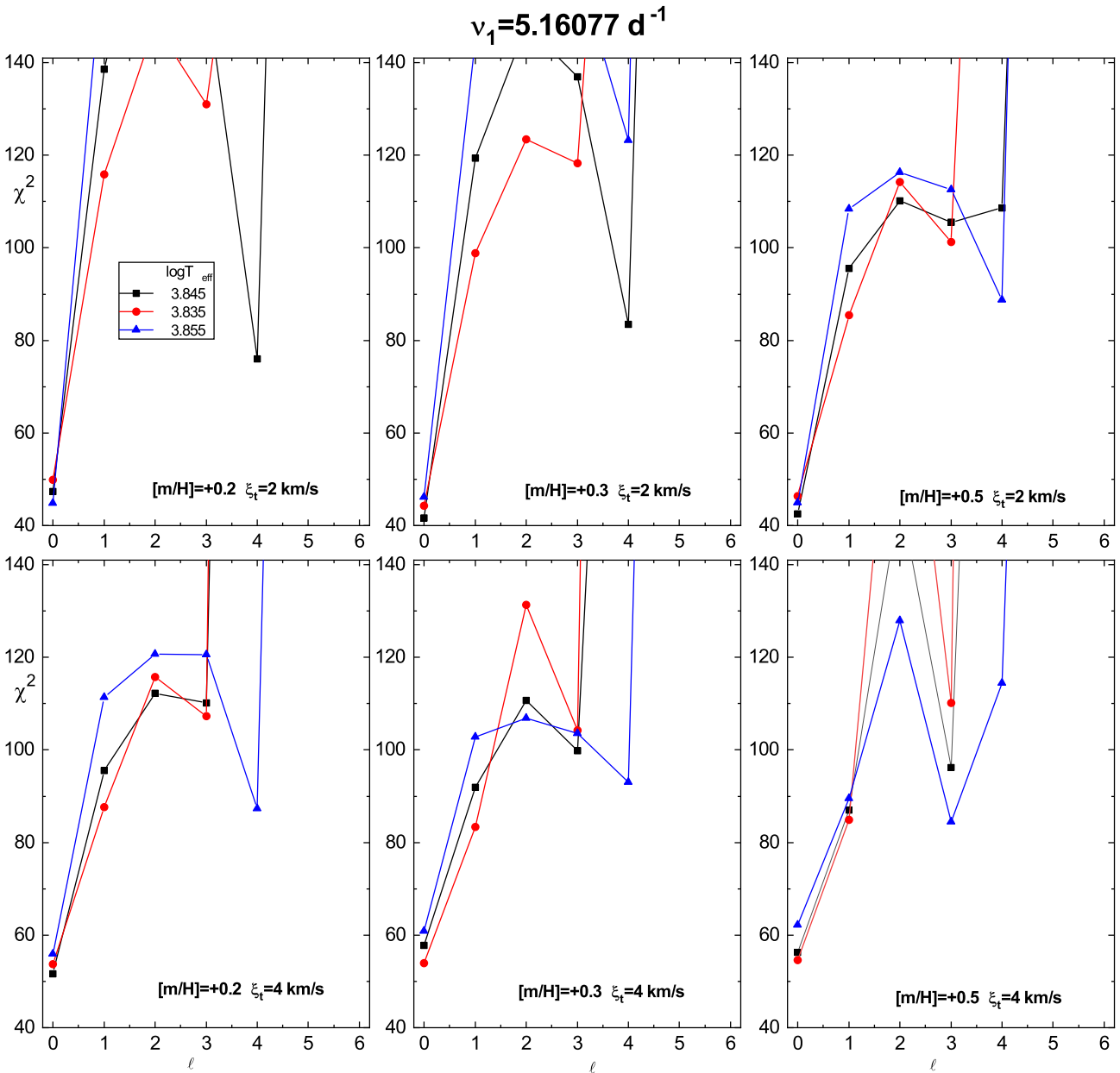
$\nu_1 = 5.16077\,\mathrm{d}^{-1}$

Figure 6. The discriminant χ^2 as a function of ℓ for the dominant frequency ν_1 for various combinations of [m/H] and ξ_t.

4, but $\ell = 4$ is indicated only by the hottest effective temperature. The frequency $\nu_8 = 8.79913\,\mathrm{d}^{-1}$ is most probably the mode $\ell = 1$, because $\ell = 5$ has much lower visibility and $\ell = 0$ is excluded because no theoretical radial overtones have frequencies close to it. In the case of $\nu_9 = 8.29217\,\mathrm{d}^{-1}$ we can only say that this is a mode with $\ell \leq 4$ and exclude $\ell = 0$ because of the frequency value.

5 MODELS FITTING THE DOMINANT FREQUENCY AS THE RADIAL MODE

Pulsational models for δ Scuti were computed with the linear non-adiabatic code of Dziembowski (1977). The code takes into account the effects of rotation up to the second order. The convective flux is assumed to be constant during the pulsational cycle; this is called the convective flux freezing approximation. This approximation is adequate if convection is not very efficient, i.e. if it does not dominate the energy transport. In the case of the efficient convection, mode

properties and driving can be affected in δ Sct star models. However, as we showed on the example of another δ Sct star FG Vir with similar parameters to δ Scuti, the results from different treatments of convection are similar for α_{MLT} less than about 1.0 (Daszyńska-Daszkiewicz et al. 2005a).

Three opacity tables were used: OPAL (Iglesias & Rogers 1996), OP (Seaton 2005), and OPLIB (Colgan et al. 2015, 2016). In the first step, we searched for models that reproduce the dominant frequency $\nu_1 = 5.16077\,\mathrm{d}^{-1}$ as a radial mode. Fig. 10 shows evolutionary tracks with such models marked on them. The dots represent the radial fundamental mode ($n = 1$) and the triangles represent the radial first overtone ($n = 2$). The models were computed with OPAL opacities but the results obtained with OP and OPLIB opacity data are qualitatively the same and quantitatively not very different. The four panels show the results computed for various combinations of X_0, Z, and α_{ov}, adopting $\alpha_{\mathrm{MLT}} = 0.5$. For the considered masses and effective temperatures, the effect of α_{MLT} is minor and, for example,
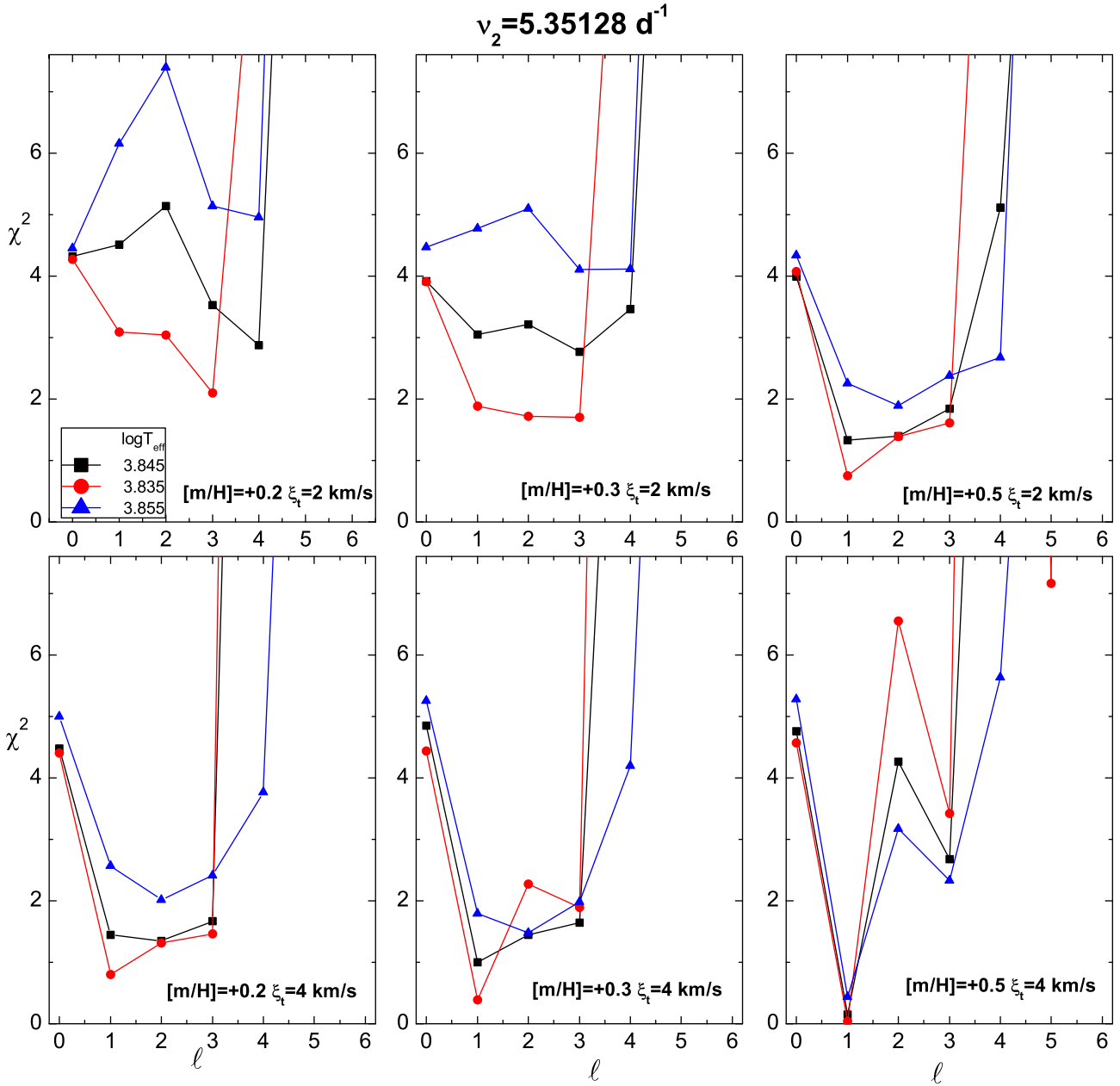
$\nu_2=5.35128\ d^{-1}$

Figure 7. The same as in Fig. 6 but for the frequency ν_2.

the models computed with $\alpha_{MLT} = 1.8$ that reproduce ν_1 as the fundamental mode have parameters that differ in value to the fourth decimal place. As one can see, in all cases the first overtone is far outside the error box of δ Sct. Therefore, we unequivocally conclude that the dominant frequency is the radial fundamental mode and thus we confirm the result of Templeton et al. (1997).

Now, let us return to the question of the evolutionary stage of δ Scuti. In case of models computed without overshooting from the convective core (the top-right panel of Fig. 10), only the post-main-sequence phase is allowed within the observational error box. It is worth to add that in case of models with the metallcity lower than $Z = 0.019$ at $\alpha_{ov} = 0.25$, the dominant mode reaches the observed value of the frequency also only in post-main-sequence stage. In case of models computed with overshooting from the convective core of $\alpha_{ov} = 0.25$ and $Z > 0.019$ (the other three panels of Fig. 10), the frequency of the radial fundamental mode can be reproduced in

the three stages of evolution: MS, OC, and post-MS. Moreover, the models in these three stages can have very similar stellar parameters ($\log T_{\rm eff}$, $\log L/L_\odot$). In Table 2, we give the parameters of such models computed for various combinations of the parameters X, Z, α_{ov} for the two values of the mixing length parameter in the envelope $\alpha_{MLT} = 0.5$ and $\alpha_{MLT} = 1.8$. In addition to these parameters, Table 2 also includes mass, the phase of evolution, effective temperature, luminosity, radius, the real and imaginary parts of the non-adiabatic parameter f of the radial fundamental mode, and the normalized work integral η. The positive value of η means that the pulsational mode is unstable (i.e. excited).

A few important conclusions can be drawn from Table 2. First, the parameter f does not differ much between the various phases of evolution and cannot be a diagnostic tool to distinguish them. The small differences in the values of f result rather from slightly various effective temperatures and luminosities. The result agree with the fact
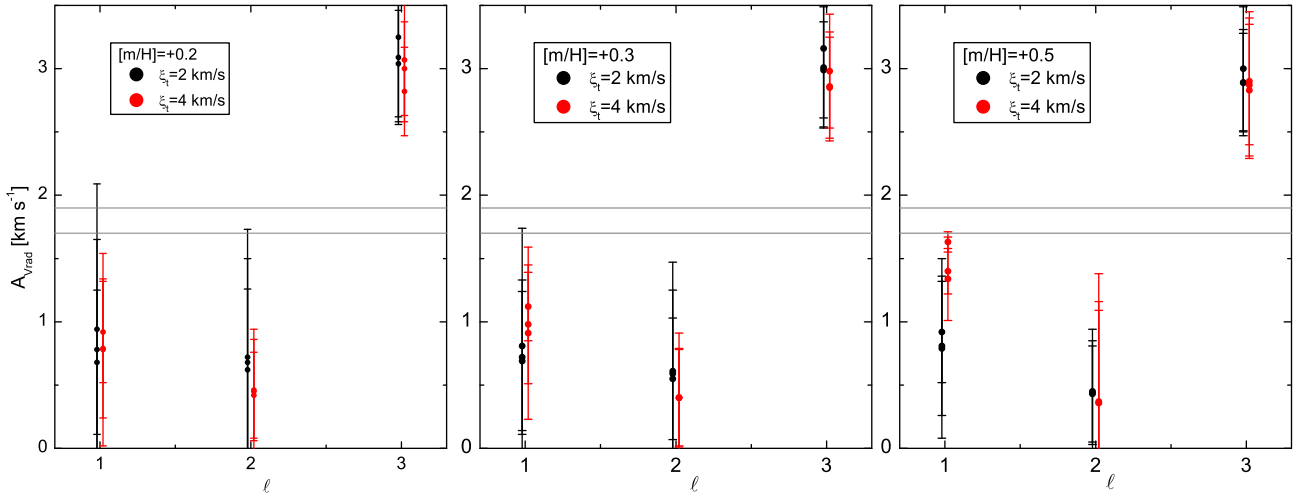
Figure 8. The estimated amplitude of the radial velocity for the second frequency ν_2 as a function of the possible mode degrees ℓ. The panels from the left to the right show the results for $[m/H] = 0.2$, 0.3, and 0.5, for the two values of ξ_t in each case. The same three values of $T_{\rm eff}$ as in Figs 6 and 7 were considered. The horizontal lines mark the observed range as determined by Balona et al. (1981).

that actually the value of f is determined entirely in subphotospheric layers, thus it mainly depends on the global parameters ($T_{\rm eff}$, $L/L_\odot$). In other words, the models with the same position in the HR diagram but in various evolutionary stages would have very similar values of f for a given pulsational mode. The major effect on the value of the parameter f comes from the efficiency of convective transport in the outer envelope, measured by the mixing length parameter $\alpha_{\rm MLT}$. As one can see from Table 2, the models computed for $\alpha_{\rm MLT} = 0.5$ and $\alpha_{\rm MLT} = 1.8$ have nearly the same effective temperatures and luminosities but the values of f for the radial fundamental mode differ enormously. This strong sensitivity is well known and can be used to derive constraints on $\alpha_{\rm MLT}$ in case of δ Sct and SX Phe pulsators if the empirical values of f are determinable from multicolour photometric variability (Daszyńska-Daszkiewicz et al. 2003, 2005a; Daszyńska-Daszkiewicz 2007; Daszyńska-Daszkiewicz et al. 2020). The next finding is that the initial hydrogen abundance X_0 and metallicity Z do not affect significantly the values of f at roughly the same effective temperature and luminosity. As for the mode instability, in each case the radial fundamental mode is excited. The effect of $\alpha_{\rm MLT}$ on the mode instability is noticeable and, in this case, the value of η is greater for higher values of $\alpha_{\rm MLT}$, i.e. for more efficient convection.

The last conclusion is that having available observables of δ Scuti, we cannot determine its evolutionary stage; it can be either the MS or post-MS star. To unravel the evolutionary stage in such case as δ Scuti, i.e. in the vicinity of TAMS, independent constraints on the mass and/or radius are necessary. Such constraints could be reached, e.g. by fitting another pulsational frequency with a plausible mode identification. Depending on the evolutionary stage, the age of δ Scuti is between about 0.82 Gyr for the main-sequence case and about 1.1 Gyr for the post-main-sequence case.

The identification of the radial order n for dipole or quadruple modes depends strongly on the evolutionary stage. In the case of the frequency $\nu_2 = 5.35128\ {\rm d}^{-1}$, identified most probably as the dipole mode, it would be the mode g_3 or g_4 in the MS or OC model, respectively. If one considers the post-MS models, then ν_2 would correspond approximately to $g_{18}...g_{22}$. To give another example, let us consider the next highest amplitude frequency in the APT data, i.e. $\nu_5 = 8.59641\ {\rm d}^{-1}$, as the dipole mode. In the MS and OC models it will be p_1 or g_1, while in the post-MS models it will be $g_8...g_{11}$.

In all cases, all these modes have mixed character with the input of the kinetic energy in the gravity propagation zone, $E_{k,g}$, to the total

kinetic energy, E_k, up to 90 per cent. In Table 3, we give the examples of the radial order identification for the models from Table 2 with $Z = 0.020$ and $Z = 0.028$ at $X_0 = 0.70$, $\alpha_{\rm ov} = 0.25$, and $\alpha_{\rm MLT} = 0.5$. For some modes, the theoretical frequencies differ quite significantly from the observed values (e.g. in the MS model with $Z = 0.02$ and the OC model with $Z = 0.028$), but one has to remember that the azimuthal order m for ν_2 and ν_3 is unknown.

6 CONSTRAINTS ON OUTER-LAYER CONVECTION

As have been already mentioned, the method of mode identification described in Section 4 provides, besides the mode degree ℓ, semi-empirical values of two complex quantities: the parameter f and the intrinsic mode amplitude ε multiplied by $Y_\ell^m(i, 0)$. As a reminder, the parameter f is the amplitude of the radiative flux variations at the level of the photosphere and ε gives the relative radius variation. These two parameters are semi-empirical because their values depend on the model atmospheres, in particular on the parameters of the metallicity $[m/H]$ and microturbulent velocity ξ_t. The quantity $\tilde{\varepsilon} = \varepsilon Y_\ell^m(i, 0)$ has been already used to make a choice between the three mode degrees for the frequency $\nu_2 = 5.35128\ {\rm d}^{-1}$. We obtained also that the dominant mode causes a change of the photospheric radius by 0.3–0.9 per cent.

Unlike ε, the empirical values of f can be directly compared with the results of linear non-adiabatic computations of stellar pulsations provided that the mode degree ℓ is uniquely identified. We started pulsational modelling with the OPAL opacity tables assuming five values of the mixing length parameter $\alpha_{\rm MLT} = 0.0, 0.5, 1.0, 1.8, 2.5$.

In Fig. 11, we show comparisons of the empirical and theoretical values of f for the two models fitting frequency ν_1 as the radial fundamental mode. The real and imaginary parts of f is denoted by f_R and f_I, respectively. The top panel shows the theoretical values of f for the model with $Z = 0.02$, $M = 2.25\ {\rm M}_\odot$, $\log T_{\rm eff} = 3.8408$, and $\log L/L_\odot = 1.571$. The corresponding empirical values are for an atmospheric metallicity $[m/H] = 0.2$, 0.3, and a microturbulent velocity $\xi_t = 2$, $4\ {\rm km\ s}^{-1}$. In the bottom panel a comparison is made for the theoretical model with the parameters: $Z = 0.028$, $M = 2.40\ {\rm M}_\odot$, $\log T_{\rm eff} = 3.8383$, $\log L/L_\odot = 1.578$, and the empirical values of f were determined for $[m/H] = 0.3, 0.5$ and $\xi_t = 2$, $4\ {\rm km\ s}^{-1}$. Both these models had an initial hydrogen abundance $X_0 = 0.70$ and
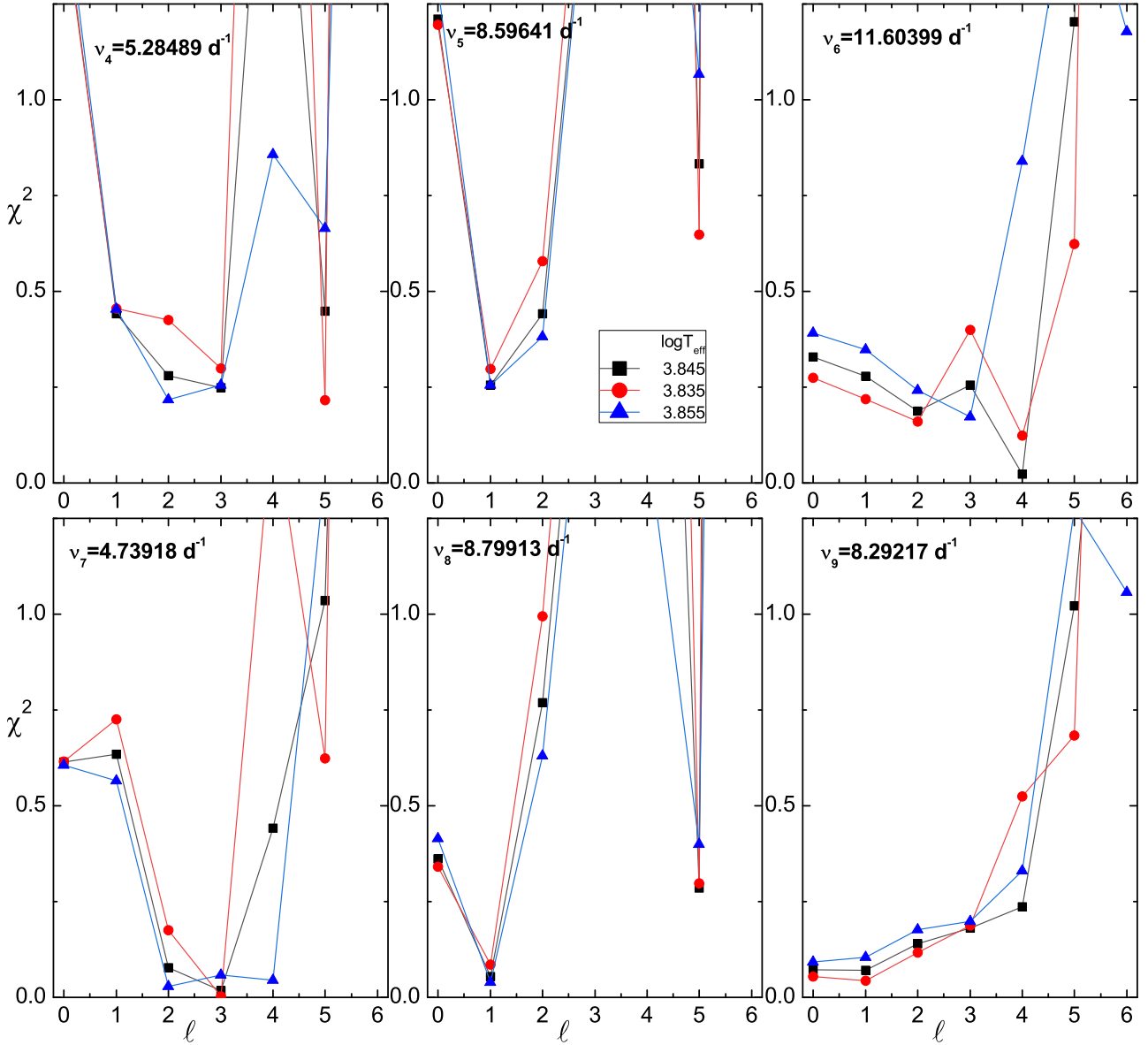
Figure 9. The value of $\chi^2(\ell)$ for the remaining six frequencies of δ Scuti for the atmospheric metallicity [m/H] = +0.5 and the microturbulent velocity $\xi_t =$ 4 km s^{-1}. The same values of the effective temperature as in Figs 6 and 7 were considered.

overshooting from the convective core $\alpha_{ov} = 0.25$. We look for models (orange dots) which are within the errors of the empirical values (black dots).

As we can see, despite the large errors in the empirical values of f, we can conclude that the efficiency of convective transport in the envelope of δ Scuti can be described by the mixing length parameter α_{MLT} less than about 1.0. This conclusion is independent of the input parameters in evolutionary computations, i.e. Z, X_0, and α_{ov}, as well as independent of T_{eff} and $\log L$ in the observed ranges of δ Scuti. On the other hand, one can see a strong effect of the atmospheric parameters, i.e. [m/H] and ξ_t, on the empirical values of f. This effect is comparable to the effect of α_{MLT} on the theoretical values of f. In case of the models computed for $Z = 0.020$ (the top panel of Fig. 11), we obtain approximately:

(i) $\alpha_{MLT} \lesssim 0.5$ for $\xi_t = 2$ km s^{-1},
(ii) $\alpha_{MLT} \lesssim 1.0$ for $\xi_t = 4$ km s^{-1}.

In the case of the models with $Z = 0.028$, we have:

(i) $\alpha_{MLT} \lesssim 0.5$ for ([m/H], ξ_t) = (0.3, 2 km s^{-1}),
(ii) $\alpha_{MLT} \lesssim 1.0$ for ([m/H], ξ_t) = (0.3, 4km s^{-1})∪(0.5, 2km s^{-1}),
(iii) $\alpha_{MLT} \in (0.5, 1.0)$ for ([m/H], ξ_t) = (0.5, 4 km s^{-1}).

Because for the pair ([m/H], ξ_t) = (0.5, 4 km s^{-1}) we obtained the most unique identification of ℓ in Section 4, we may infer, cautiously, that the most likely range of α_{MLT} is (0.5, 1.0). None the less, regardless of the evolutionary and atmospheric parameters, we can conclude that the mixing length parameter α_{MLT} in the outer layers of δ Scuti is less than about 1.0.

Now the question is how this constraint on α_{MLT} depends on the adopted opacity data. To study this effect we computed pulsational models that reproduce the dominant frequency of δ Scuti as the radial fundamental mode adopting the OP tables (Seaton 2005) and OPLIB data (Colgan et al. 2016). In Fig. 12, we show the values of f for all three sources of the opacity data for $X_0 = 0.70$, $Z = 0.028$, and α_{ov}
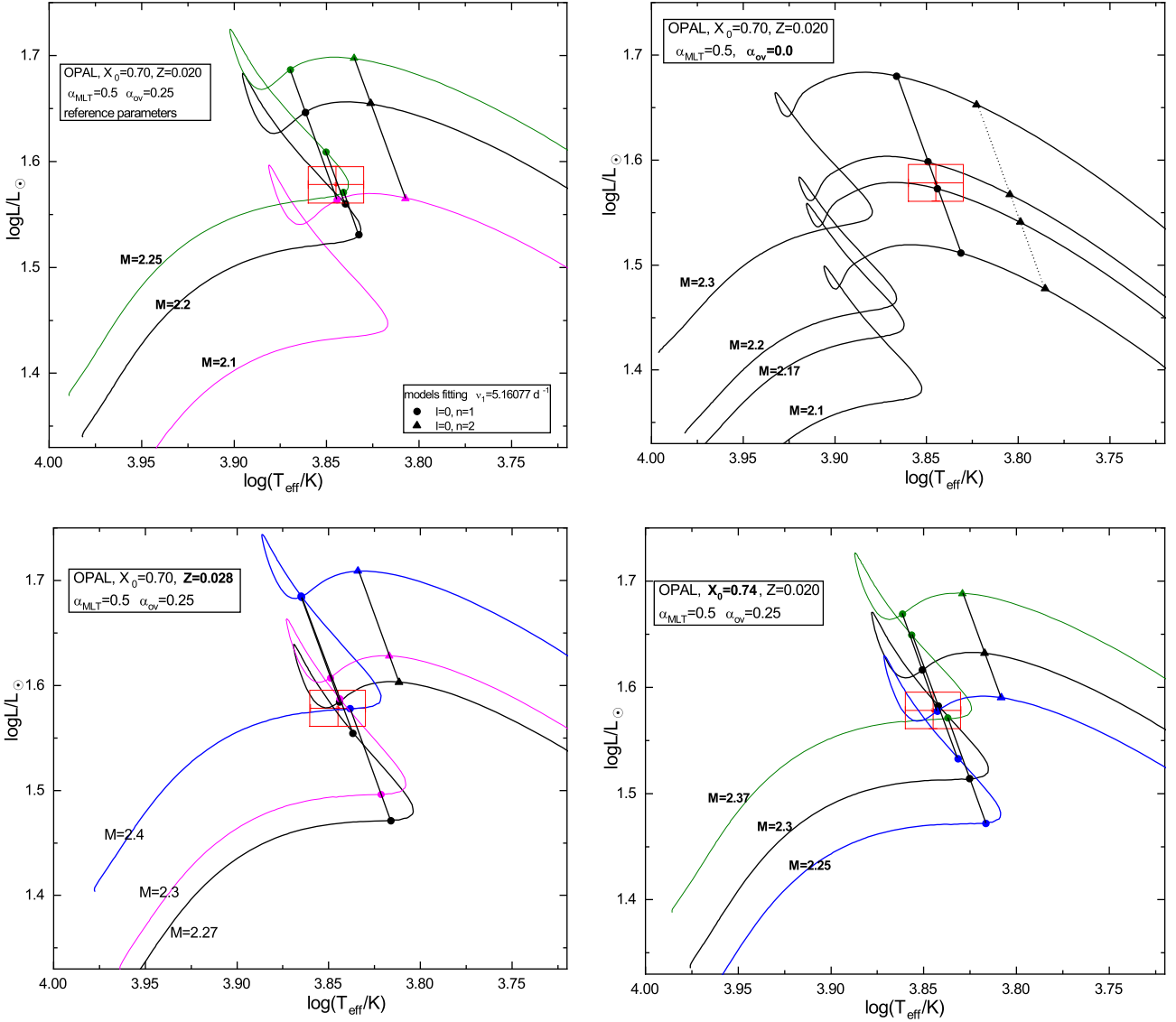
Figure 10. The OPAL evolutionary tracks with models marked as dots or triangles that reproduce the dominant frequency of δ Scuti $\nu_1 = 5.16077 \, d^{-1}$ as a radial mode. Dots correspond to the fundamental mode and triangles to the first overtone mode. The observed parameters of δ Scuti are depicted together with their error box. Each of the four panels show results for various combinations of the initial hydrogen amount X_0, metallicity Z, and overshooting from the convective core α_{ov}. A mixing length parameter in the envelope of $\alpha_{MLT} = 0.5$ was adopted in each case. The top-right panel is for the no-overshooting case.

= 0.25. The stellar parameters of these models slightly change for various values of α_{MLT} but the differences are in the fourth decimal place and the average stellar parameters are as follows:

(i) **OPAL**: $M = 2.40 \, M_\odot$, $\log T_{eff} = 3.8383$, $\log L/L_\odot = 1.578$,
(ii) **OP**: $M = 2.40 \, M_\odot$, $\log T_{eff} = 3.8379$, $\log L/L_\odot = 1.576$,
(iii) **OPLIB**: $M = 2.42 \, M_\odot$, $\log T_{eff} = 3.8378$, $\log L/L_\odot = 1.580$.

The parameters of the OPAL model are the same as in the lower panel of Fig. 11 but for a direct comparison we repeated them. The empirical values of f plotted in Fig. 12 are also the same as in the lower panel of Fig. 11 and the differences in their values for the above-mentioned parameters of the OP and OPLIB models are 10 per cent at most. Therefore, for the sake of clarity, we did not plot all empirical values of f.

The consistency of the theoretical values of f in the models of δ Scuti for the different opacity tables is striking. This result is opposite to what we obtained for B-type pulsators in our several

studies (e.g. Daszyńska-Daszkiewicz, Dziembowski & Pamyatnykh 2005b; Daszyńska-Daszkiewicz et al. 2017; Walczak et al. 2019). Thus, independently of the adopted opacities the constraints on the values of α_{MLT} remain unchanged.

Finally, we examined the effect of the chemical mixture as the atmospheric abundances of δ Scuti are anomalous. Such a check is important because the values of f are determined in the subphotospheric layers. In Fig. 13, we compare the values of f of the OPAL models computed with the AGSS09 mixture and the δ Sct mixture as determined by Yushchenko et al. (2005). As in Fig. 12, we adopted $X_0 = 0.70$, $Z = 0.028$, and $\alpha_{ov} = 0.25$ The stellar parameters of the OPAL model obtained with the δ Sct mixture, which fit the frequency of the dominant mode, are:

(i) **OPAL(δ Sct)**: $M = 2.38 \, M_\odot$, $\log T_{eff} = 3.8385$, $\log L/L_\odot = 1.577$

Table 2. The parameters of the OPAL models that reproduce $\nu_1 = 5.16077\,\mathrm{d}^{-1}$ as the radial fundamental mode ($\ell = 0$, $n = 1$). The following parameters are given in the subsequent columns: the initial hydrogen abundance X_0, metallicity Z, the overshooting from the convective core α_{ov}, mass, phase of evolution, age, effective temperature, luminosity, radius, the real and imaginary part of the non-adiabatic parameter f of the radial fundamental mode and the normalized instability parameter η. Most of the results are for $\alpha_{\mathrm{MLT}} = 0.5$ and, for a comparison, at the very bottom of the table we give the results for $\alpha_{\mathrm{MLT}} = 1.8$ at $X_0 = 0.70$, $Z = 0.020$, $\alpha_{\mathrm{ov}} = 0.25$. For $\alpha_{\mathrm{ov}} = 0.0$ only the post-MS phase is possible.

X_0	Z	$\alpha_{\mathrm{MLT}} = 0.5$ α_{ov}	$M/M_\odot$	phase	age [Gyr]	$\log T_{\mathrm{eff}}/\mathrm{K}$	$\log L/L_\odot$	$R/R_\odot$	f_R	f_I	η
0.70	0.014	0.25	1.97	post-MS	1.0617	3.8475	1.560	4.07	0.757	-12.217	0.056
0.70	0.017	0.25	2.04	post-MS	1.0574	3.8462	1.564	4.11	0.712	-12.185	0.054
0.70	0.020	0.25	2.25	MS	0.8422	3.8408	1.571	4.25	2.324	-10.656	0.071
			2.20	OC	0.9218	3.8398	1.560	4.21	2.640	-10.180	0.075
			2.10	post-MS	1.0597	3.8443	1.564	4.14	1.070	-11.840	0.057
0.70	0.020	0.00	2.17	post-MS	0.8218	3.8440	1.573	4.19	1.171	-11.845	0.057
0.70	0.028	0.25	2.40	MS	0.8154	3.8383	1.578	4.33	2.253	-10.770	0.067
			2.30	OC	0.9859	3.8439	1.587	4.27	0.178	-12.657	0.042
			2.27	post-MS	1.0252	3.8441	1.584	4.25	0.038	-12.725	0.041
0.74	0.020	0.25	2.37	MS	0.8878	3.8370	1.571	4.32	2.781	-9.988	0.074
			2.30	OC	1.0178	3.8422	1.582	4.28	0.964	-12.185	0.052
			2.25	post-MS	1.0857	3.8426	1.578	4.24	0.778	-12.277	0.050
0.70	0.020	$\alpha_{\mathrm{MLT}} = 1.8$ 0.25	2.25	MS	0.8422	3.8411	1.571	4.24	2.837	-0.172	0.104
			2.20	OC	0.9218	3.8403	1.560	4.20	2.705	-0.141	0.108
			2.10	post-MS	1.0597	3.8446	1.564	4.14	3.329	-0.465	0.096

Table 3. An assignment of the radial order n to the frequencies ν_2 and ν_3, assuming they are the $\ell = 1$ modes, for the two OPAL models from Table 2 with the metallicity $Z = 0.020$ and $Z = 0.028$. The other parameters are $X_0 = 0.7$, $\alpha_{\mathrm{ov}} = 0.25$, and $\alpha_{\mathrm{MLT}} = 0.5$. The following columns contain the evolutionary phase, mass, the symbol of the observed frequency, the values of the closest theoretical frequency in the model, mode type, the ratio of $E_{k,\,g}$ to E_k, and the instability parameter η.

Phase	M [$M_\odot$]	$Z = 0.020$ Observed frequency	Model frequency [d^{-1}]	Mode type	$E_{k,\,g}/E_k$	η
MS	2.25	ν_2	5.6732	g_3	0.83	0.081
		ν_5	8.6384	p_1	0.06	0.120
OC	2.20	ν_2	5.3916	g_4	0.65	0.085
		ν_5	8.6812	p_1	0.11	0.124
post-MS	2.10	ν_2	5.3397	g_{22}	0.56	0.057
		ν_5	8.6754	g_{11}	0.56	0.119
Phase	M [$M_\odot$]	$Z = 0.028$ Observed frequency	Model frequency [d^{-1}]	n	$E_{k,\,g}/E_k$	η
MS	2.40	ν_2	5.2644	g_3	0.19	0.072
		ν_5	8.4742	p_1	0.32	0.115
OC	2.30	ν_2	5.8684	g_4	0.89	0.061
		ν_5	8.5567	g_1	0.34	0.110
post-MS	2.27	ν_2	5.3362	g_{18}	0.71	0.047
		ν_5	8.7541	g_8	0.41	0.114

As one can see, the effect of the chemical mixture is even more negligible than when using different opacity tables.

The above results validate the obtained limits on the efficiency of convection in the δ Scuti envelope. Moreover, almost in all models the radial fundamental mode is excited. The exceptions are the OPAL and OPLIB models with a mixing length parameter $\alpha_{\mathrm{MLT}} = 2.5$.

7 CONCLUSIONS

The aim of this work was to present an extended analysis of the pulsating star δ Scuti, the class prototype that is far too little observed and studied. We analysed new multicolour time-series photometry of the star in order to extract the pulsational frequencies and, then, to identify their mode degrees. Applying Fourier analysis to the 7-yr SMEI data we extracted 18 significant frequencies with 14 being independent. No low-frequency peaks were found that could correspond to high-order gravity modes. In the combined *uvy* APT data, we detected only 10 out of 18 SMEI peaks and no other signals. Eight APT frequencies are independent and correspond to the highest amplitude SMEI peaks but $\nu_3 = 8.376999\,\mathrm{d}^{-1}$. A reanalysis of the data from Templeton et al. (1997) revealed nine significant frequencies with one undetected in the SMEI and APT observations. The third highest amplitude frequency $\nu_3 = 8.376999\,\mathrm{d}^{-1}$ detected in SMEI was also not present in Templeton et al.'s data. The lack of frequency ν_3 in the APT and Templeton et al. data proves a huge change in the amplitude of this pulsation mode.

Having the amplitudes and phases in three passbands, i.e. the Strömgren *uvy*, we made an attempt to identify the harmonic degree ℓ of the detected modes in δ Scuti, using the method of Daszyńska-Daszkiewicz et al. (2003). To this end we used Vienna model atmospheres that take into account turbulent convection. We obtained that the dominant frequency is unequivocally a radial mode as already has been suggested by, e.g. Balona et al. (1981), Cugier & Monier (1993), and Templeton et al. (1997).
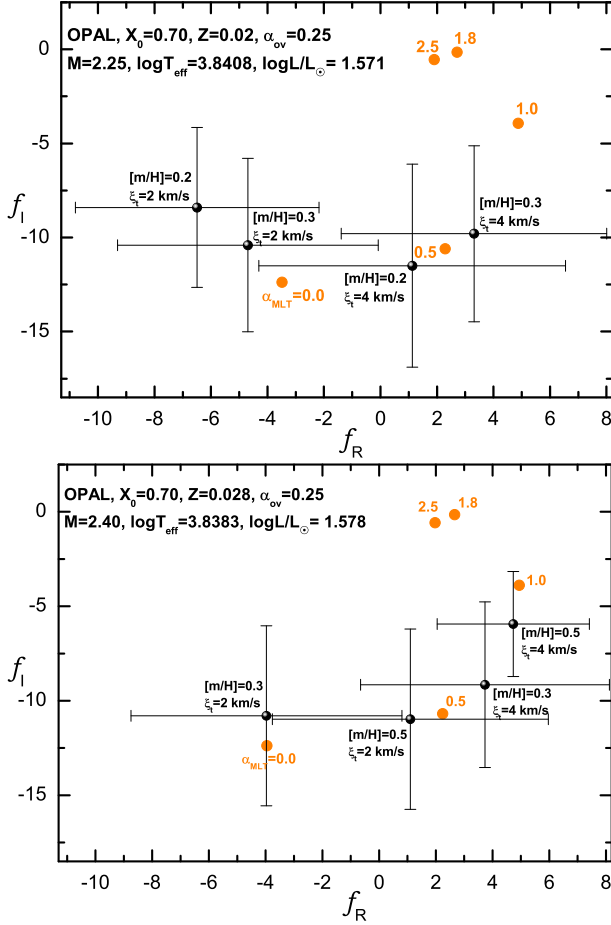
Figure 11. A comparison of the theoretical and empirical values of the non-adiabatic parameter f for the two OPAL models that reproduce the dominant frequency as the radial fundamental mode. The theoretical values of f were computed for five values of the mixing length parameter $\alpha_{MLT} = 0.0$, 0.5, 1.0, 1.8, and 2.5 (orange dots). The top panel shows the results for $Z = 0.020$ and the bottom panel for $Z = 0.028$. The parameters of the models are given in the text. The empirical values are shown for the atmospheric metallicity $[m/H] = 0.2$, 0.3 (the top panel) and $[m/H] = 0.3$, 0.5 (the bottom panel). Two values of the microturbulent velocity ξ_t were adopted in each case.

δ Scuti is quite abundant in metals with a measured value of metallicity $[m/H] \in (0.18, 0.38)$. It is also considered as a chemical peculiar star with an excess of such elements as aluminium, iron, nickel, and manganese. This is probably a reason why the goodness of the fit of the calculated amplitudes and phases to the observed values are so sensitive to the adopted metallicity $[m/H]$ and microturbulent velocity ξ_t. This sensitivity is even stronger for the lower amplitude frequencies. The most homogenous fit in the whole observed range of T_{eff} was obtained for $[m/H] = +0.5$ and $\xi_t = 4$ km s^{-1}. In other words, for these atmospheric parameters the discriminant χ^2 has a similar dependence on the effective temperature and mode degree ℓ. We determined that frequency ν_2 is most probably an $\ell = 1$ mode and the other six frequencies have far less unique identifications of ℓ. The identification of $\ell = 1$ for ν_2 was also verified by comparing the estimated amplitude of the radial velocity change with the observed value as derived by Balona et al. (1981). This assessment has been done by adopting the empirical values of $\tilde{\varepsilon} \equiv \varepsilon Y_\ell^m(i, 0)$ as determined from our method. Moreover, for the dominant frequency ν_1, which is a radial mode, we could estimate the intrinsic amplitude itself, i.e.
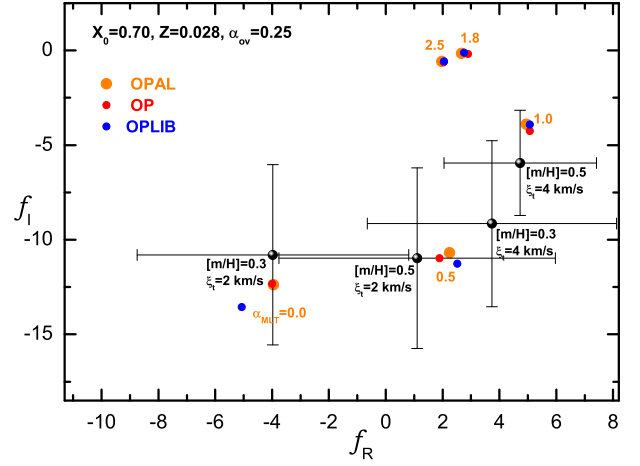

Figure 12. The same as in the bottom panel of Fig. 11, but the result for the OP and OPLIB models with very close stellar parameters were added.
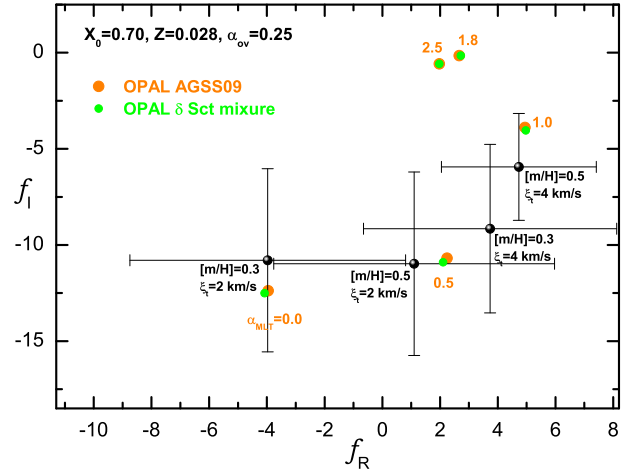

Figure 13. The same as in the bottom panel of Fig. 11, but the result for the OPAL models computed with the δ Scuti mixture adopted from Yushchenko et al. (2005) were added.

ε. The result is that the changes of the radius caused by the dominant mode are between 0.3 per cent and 0.9 per cent.

In the next step, we constructed the pulsational models that reproduce the dominant frequency as the radial fundamental or first overtone modes. It appeared that in the allowed range of $(T_{eff}, L/L_\odot)$, the frequency ν_1 can be associated only with the fundamental mode, which confirms Templeton et al.'s result. The pulsational models with ν_1 as the first overtone are far outside the error box and all are in the post-main-sequence phase. In the case of the radial fundamental mode, three phases of evolution are possible: main sequence, overall contraction, and post-main-sequence stage. However, for the star to be on the main sequence, the convective overshooting parameter, α_{ov}, must be at least 0.25 for the metallicity greater than $Z = 0.019$.

Unfortunately, we do not have any diagnostic tool that can distinguish what the actual evolution phase of δ Scuti is. For example, it turned out that the value of the non-adiabatic parameter f is determined by the effective temperature and the luminosity, i.e. by the position of the star in the HR diagram. Moreover, there are no more frequencies with a firm identification of (ℓ, m) that could better constrain our seismic models. Thus, we are left with the open question of whether this prototype is a main-sequence

or post-main-sequence star. In the considered range of the initial hydrogen abundance X_0 and metallicity Z, our estimate of the age of δ Scuti is about 0.82–0.89 Gyr for the main-sequence phases, about 0.92–1.02 Gyr for the overall contraction, and about 1.02–1.09 Gyr for the post-main-sequence phase.

One of the main results of this work are constraints on the efficiency of convective transport in the envelope of δ Scuti, on the assumption of the frozen convection approximation. This has been done by comparing the empirical and theoretical values of the parameter f for the dominant radial mode. Our results testify in favour of rather low to moderately efficient convection in the outer layers, described by a mixing length parameter α_{MLT} less than 1.0, which is significantly lower than the solar value $\alpha_{\mathrm{MLT}} = 1.8$. These constraints on α_{MLT} are independent of the commonly used opacity data as the same result was obtained with all three opacity tables: OPAL, OP, and OPLIB. This weak sensitivity of f on the adopted opacity data is contrary to what we have learned from our studies of B-type pulsators (e.g. Daszyńska-Daszkiewicz et al. 2005b, 2017; Walczak et al. 2019). Moreover, the effect of the chemical mixture is completely negligible.

Unambiguous identification of the mode degree ℓ for more frequencies of δ Scuti could also help to further refine the parameter α_{MLT}. That requires more multicolour photometric observations. Besides, a simultaneous spectroscopic campaign would allow to detect more frequencies, to improve mode identification, including determination of the azimuthal order m, and to constrain the atmospheric metallicity [m/H] and microturbulent velocity ξ_t for a better comparison of the theoretical and empirical values of f.

Finally, experience with space photometry of other δ Scuti stars suggests that low-frequency oscillations would likely as well be detected in δ Scuti itself. Then, a more comprehensive seismic study could be carried out to explain the excitation of high-order gravity modes and possibly to achieve constraints on the mean opacity profile.

ACKNOWLEDGEMENTS

DATA AVAILABILITY

The APT observations as well as theoretical computations will be shared on reasonable request to the corresponding author.

REFERENCES

Antoci V. et al., 2019, MNRAS, 490, 4040
Asplund M., Grevesse N., Sauval A. J., Scott P., 2009, ARA&A, 47, 481
Balona L. A., 1994, MNRAS, 268, 119
Balona L. A., Dean J. F., Stobie R. S., 1981, MNRAS, 194, 125

Balona L. A., Daszyńska-Daszkiewicz J., Pamyatnykh A. A., 2015, MNRAS, 452, 3073
Boeche C., Grebel E. K., 2016, A&A, 587, 2
Bowman D. M., Kurtz D. W., 2018, MNRAS, 476, 3169
Bowman D. M., Kurtz D. W., Breger N., Murphy S. J., Holdsworth D. L., 2016, MNRAS, 460, 1970
Breger M., Pamyatnykh A. A., 1998, A&A, 332, 958
Breger M., Pamyatnykh A. A., 2006, MNRAS, 368, 571
Breger M. et al., 2005, A&A, 435, 955
Campbell W. W., Wright W. H., 1900, ApJ, 12, 254
Canuto V. M., Goldman I., Mazzitelli I., 1996, ApJ, 473, 550
Chevalier C., 1971, A&A, 14, 24
Claret A., 2000, A&A, 363, 1081
Colgan J., Kilcrease D. P., Magee N. H., Abdallah J., Sherrill M. E., Fontes C. J., Hakel P., Zhang H. L., 2015, High Energy Density Phys., 14, 33
Colgan J. et al., 2016, ApJ, 817, 116
Cugier H., Monier R., 1993, Acta Astron., 43, 39
Daszyńska-Daszkiewicz J., 2007, Comm. Asteroseismol., 150, 32
Daszyńska-Daszkiewicz J., Dziembowski W. A., Pamyatnykh A. A., 2003, A&A, 407, 999
Daszyńska-Daszkiewicz J., Dziembowski W. A., Pamyatnykh A. A., Breger M., Zima W., Houdek G., 2005a, A&A, 438, 653
Daszyńska-Daszkiewicz J., Dziembowski W. A., Pamyatnykh A. A., 2005b, A&A, 441, 641
Daszyńska-Daszkiewicz J., Pamyatnykh A. A., Walczak P., Colgan J., Fontes C. J., Kilcrease D. P., 2017, MNRAS, 466, 2284
Daszyńska-Daszkiewicz J., Pamyatnykh A. A., Walczak P., Szewczuk W., 2020, MNRAS, 499, 3034
Dziembowski W. A., 1977, Acta Astron., 27, 95
Erspamer D., North P., 2003, A&A, 398, 1121
Eyles C. J. et al., 2003, Solar Phys., 217, 319
Ferguson J. W., Alexander D. R., Allard F., Barman T., Bodnarik J. G., Hauschildt P. H., Heffner-Wong A., Tamanai A., 2005, ApJ, 623, 585
Gaia Collaboration, 2021, A&A, 649, A1
Gray R. O., Napier M. G., Winkler L. I., 2001, AJ, 121, 2148
Grevesse N. M., Sauval A. J., 1998, Space Sci. Rev., 85, 161
Grigahcéne A. et al., 2010, ApJ, 713L, 192
Guzik J. A., Garcia J. A., Jackiewicz J., 2019, Front. Astron. Space Sci., 6, 40
Heiter U. et al., 2002, A&A, 392, 619
Holmberg J., Nordstrom B., Andersen J., 2009, A&A, 501, 941
Iglesias C. A., Rogers F. J., 1996, ApJ, 464, 943
Jackson B. V. et al., 2004, Solar Phys., 225, 177
Marconi M., Palla F., 1998, ApJ, 507, L141
Masana E., Jordi C., Maitzen H. M., Torra J., 1998, A&AS, 128, 265
Moskalik P. A., 1985, Acta Astron., 35, 229
Murphy S. J., Hey D., Van Reeth T., Bedding T. R., 2019, MNRAS, 485, 2380
Pamyatnykh A. A., 1999, Acta Astron., 49, 119
Pamyatnykh A. A., Dziembowski W. A., , Handler G., Pikall H., 1998, A&A, 333, 141
Paunzen E., 2015, A&A, 580, 23
Poretti E. et al., 2009, A&A, 506, 85
Rogers F. J., Nayfonov A., 2002, ApJ, 576, 1064
Rogers F. J., Swenson F. J., Iglesias C. A., 1996, ApJ, 456, 902
Rosner B., 1983, Technometrics, 25, 165
Schroeder C., Reiners A., Schmitt H. M. M., 2009, A&A, 493, 1099
Seaton M. J., 2005, MNRAS, 362, L1
Templeton M. R., McNamara B. J., Guzik J. A., Bradley P. A., Cox A. N., Middleditch J., 1997, AJ, 114, 1592
Torres G., 2010, AJ, 140, 1158
Walczak P. et al., 2019, MNRAS, 485, 3544
Yushchenko A., Gopka V., Kim C., Musaev F., Kang Y. W., Kovtyukh V., Soubiran C., 2005, MNRAS, 359, 865
Zwintz K. et al., 2014, Science, 345, 550

This paper has been typeset from a T$_{\rm E}$X/L$^{\rm A}$T$_{\rm E}$X file prepared by the author.